International Journal of Thermophysics, Vol. 24, No. 5, September 2003 (© 2003)

The Viscosity Surfaces of Propane in the Form of Multilayer Feed Forward Neural Networks[1]

G. Scalabrin[2, 3] and G. Cristofoli[2]

The present work focuses on the development of a viscosity equation $\eta = \eta(\rho, T)$ for propane through a *multilayer feedforward neural network* (MLFN) technique. Having been successfully applied to a variety of fluids so far, the proposed technique can be regarded as a general approach to viscosity modeling. The MLFN viscosity equation has been based on the available experimental data for propane: validation on the 969 primary data shows an average absolute deviation (AAD) of 0.29% in the temperature, pressure, and density range of applicability, i.e., 90 to 630 K, 0 to 60 MPa, and 0 to 730 $kg \cdot m^{-3}$. This result is very promising, especially when compared with experimental data uncertainty. The minimum amount of required data for setting up the MLFN has been investigated, to explore the minimum cost of the model. Comparisons with other viscosity models are presented regarding amount of input data, claimed accuracy, and range of applicability, with the aim of providing a guideline when viscosity has to be calculated for engineering purposes. A high accuracy equation of state for the conversion of variables from experimental P, T to operative ρ, T has to be provided. To overcome this requirement, two viscosity explicit equations in the form $\eta = \eta(P, T)$ are also developed, for the liquid and for the vapor phases. The respective AADs are 0.58 and 0.22%, comparable with those of the former $\eta = \eta(\rho, T)$ equation. Finally, the trend of the experimental viscosity second virial coefficient is reproduced and compared with that obtained from the MLFN.

KEY WORDS: feedforward neural networks; heuristic techniques; propane; viscosity.

[1] Paper presented at the Sixteenth European Conference on Thermophysical Properties, September 1–4, 2002, London, United Kingdom.

[2] Dipartimento di Fisica Tecnica, Università di Padova, via Venezia 1, I-35131 Padova, Italy.

[3] To whom correspondence should be addressed. E-mail: gscala@unipd.it

0195-928X/03/0900-1241/0 © 2003 Plenum Publishing Corporation

1. INTRODUCTION

The state of the art for viscosity surface representation, on which the present work focuses, suggests at least two approaches. First, predictive or semipredictive models can be used. These models are often based on corresponding states theory [1–7] and, in many cases, they are capable of estimating the property with an accuracy level sufficient for engineering calculations.

Alternatively, conventional viscosity equations can be used, which are based on the residual concept superimposing three parts: the dilute-gas, the excess terms, and the critical enhancement. This technique is essentially correlative and requires experimental data as evenly distributed as possible over the entire thermodynamic $P\rho T$ surface. It usually leads to an equation in the form $\eta = \eta(\rho, T)$. Since the viscosity data are inevitably related to the experimentally-accessible (T, P) variables, an equation of state is needed to convert (T, P) to (T, ρ). Moreover, viscosity data at pressures approaching zero have to be extrapolated to fit the coefficients of the dilute-gas term in the viscosity equation. Because the final correlation relies only on the available data, this poses the question of whether a completely empirical correlation $\eta = \eta(\rho, T)$ could be developed directly from data alone.

The aim of the present work is to develop two viscosity equations, the first in T, ρ and the second in T, P variables, directly based on experimental data through a *multilayer feedforward neural network* (MLFN), which can be considered as one of the most powerful and flexible regression techniques for function approximation.

The study is devoted to propane, for which a conventional dedicated viscosity equation has already been developed by Vogel et al. [9], thus enabling comparison of the results. So far the MLFN approach has been successfully applied to R123 [10], R134a [11], ethane [12], R152a [13], and now propane; as a consequence, the present technique can be regarded as a general tool for viscosity calculations.

2. CONVENTIONAL VISCOSITY EQUATION FOR PROPANE

Vogel et al. [9] developed a dedicated viscosity equation for propane using the conventional procedure base on the residual concept [14]:

$$\eta(\rho, T) = \eta_0(T) + \Delta\eta_R(T, \rho) + \Delta\eta_C(T, \rho) \tag{1}$$

where $\eta_0(T)$ is the dilute-gas term representing the zero-density limit of gas viscosity and $\Delta\eta_R(T, \rho)$ is the residual or excess function for the calculation

of which the dilute-gas and the critical enhancement terms must be subtracted from the actual viscosity value.

In the dilute-gas region data are needed in the lower density zone in order to extrapolate to the zero-density values. Isothermal data are collected and regressed through a linear fit, where on the x-axis density is reported while the y-axis represents viscosity. As will be shown later, the slope is related to the second virial viscosity coefficient while the intercepts at $\rho = 0$ for different temperatures are used to regress the coefficients of the zero-density viscosity function, upon which the form is theoretically based.

The critical enhancement term $\Delta\eta_C(T, \rho)$ describes the behavior of a fluid in the critical region, where the transport properties are influenced by long-range fluctuations. The critical enhancement of the transport properties can be described by a crossover theory [15, 16]. Since this term has only a modest influence on viscosity and only when very close to the critical point and since data in the critical region are lacking, the term is not taken into account for propane.

The excess term describes the density dependence. While the zero-density function is theoretically sound, this term is purely empirical, since both the analytical form and the coefficients have to be optimized. For this purpose, as many data as possible are required.

To convert the (T, P) variables to (T, ρ), Vogel et al. adopted a MBWR 32-term equation of state [17]; the accuracy of the converting equation is critical, since a small error in density can propagate to significant deviations when used in the viscosity correlation. In the dense phase an error of 0.1% can lead to a viscosity error of 10%, as can easily be seen from a sensitivity analysis of the viscosity equations. The validity ranges of that viscosity equation are $90 \leqslant T \leqslant 478$ K and $P \leqslant 62$ MPa.

During the development of the present work a further multiparameter equation of state in the form of the dimensionless Helmholtz free energy has been made available for propane in the literature [60], but it was anyway proved that the small increase of volumetric accuracy introduced by this equation could not affect the global results obtained with the present formulation.

3. NEURAL NETWORKS

In the preceding sections it was pointed out that:

1. Even though the structure of the conventional viscosity equation sounds theoretically well-based, experimental data distributed over the whole $P\rho T$ surface are needed in order to regress the coefficients of the three contributions;

2. It is by no means easy to find the most suitable analytical form for representing the density and temperature dependence of the residual term: it is not only a matter of parameters to fit but moreover a matter of optimizing the excess term analytical form;
3. The fitting procedure is not straightforward; data have to be converted in order to split the influences of the three terms;
4. A highly accurate equation of state is needed for converting the measured variables (T, ρ) into (T, P).

Because experimental data covering the whole $P\rho T$ surface are needed for the development of a conventional viscosity equation dedicated to a target fluid, it seems reasonable to test a single correlative technique based directly on all available data. Clearly, the analytical form of the new model has to be highly flexible in fitting the experimental viscosity surface of a generic fluid. It cannot be an equation with a number of parameters to regress because such a form may be too rigid and not suitable to be forced on the experimental data. From previous experience, i.e., for R134a [11], at low density viscosity may show an inversion point: it decreases to some extent and then it increases to the zero-density limit. A simple polynomial form, for example, cannot accurately represent such low-density behavior, unless a poor representation in the high-dense phase is accepted. During the preliminary stages, it was established that neural networks, applied as function approximators, have demonstrated the required characteristics to a high degree once applied to a viscosity surface. Reference is made to the cases for R123 [10], R134a [11], ethane [12], and R152a [13] to which this new procedure has been successfully applied.

A new correlation technique is then proposed here, based on neural networks. The heart of the problem is to approximate the viscosity function by fitting the available data. What is called "training" in the neural network reference literature is here a classical optimization problem requiring the regression of viscosity data to obtain the "weighting factors," i.e., the coefficients of the function.

Among different neural network architectures, *a multilayer feedforward neural network* (MLFN) with only one hidden layer seems to be the most effective as a universal approximator of continuous functions in a compact domain [18–20]. In this architecture there are several neuron layers *(multilayer)* and information goes in one direction only, from input to output *(feedforward)*, i.e., from left to right in Fig. 1. This figure shows the general architecture of a MLFN with a hidden layer, which is the analytical tool used in the present work as a viscosity equation model.

Referring to Fig. 1, the two values of the input layer, U_1 and U_2, represent the independent variables. The independent variables U_1 and U_2

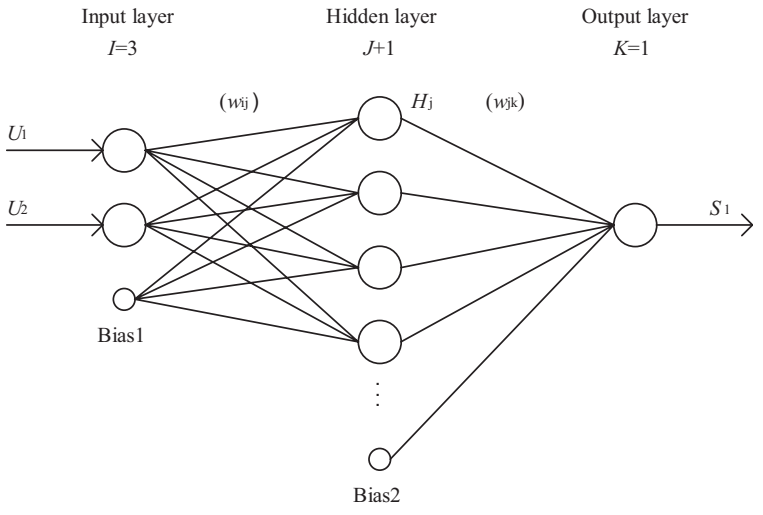

Fig. 1. General architecture of a MLFN.

then feed the hidden layer, made by $J+1$ nodes or neurons. The output of each neuron H_j is

$$H_j = f\left(\sum_{i=1}^{I} w_{ij} U_i\right) \tag{2}$$

where w_{ij} are the weights applied to the H_j neuron input information, I is the number of input, and f is the transfer function,

$$f(x) = \alpha \frac{1}{1+e^{-2\beta x}} \tag{3}$$

with

$$x = \sum_{i=1}^{I} w_{ij} U_i \tag{4}$$

Two positive parameters have been applied in Eq. (3) to make the function's behavior more flexible; α changes the activation span, and β determines the steepness of the sigmoid function. In this work they are set, respectively, to 1.0 and 0.005. What happens is that each neuron of a layer makes the weighted summation of all the neurons in the previous layer, and then passes this summation through a transfer function.

The outputs of the hidden layer feed the output layer such that

$$S_k = f\left(\sum_{j=1}^{J+1} w_{jk} H_j\right) \tag{5}$$

where again f is the transfer function, Eq. (3), w_{jk} are the weights applied to the S_k neuron output information, and J is the number of hidden neurons in the hidden layer.

Two more neurons are added to the input and to the hidden layers: *Bias* 1 and *Bias* 2. They are needed to accelerate the regression of the weighting factors. In this work they are both set to 1.0.

$$U_3 = Bias\ 1 \tag{6}$$

$$H_{J+1} = Bias\ 2 \tag{7}$$

If MLFN is applied to represent viscosity, then inputs U_1 and U_2 are, respectively, temperature and density, while output S is viscosity. The only unknown is the weighting factor set that can be regressed from experimental data, in the so-called training step.

The MLFN topology is determined once the number of neurons in the three layers is fixed: I represents the number of neurons in the input layer (comprehensive of a bias term), and K represents the number of neurons in the output layer. In our case, there are two physical inputs and one physical output, so $I = 3$ and $K = 1$.

The number of neurons in the hidden layer J (bias not included) has to be found by trial-and-error. The greater the J value, the better the accuracy but also the lower the computational speed and the more likely the overfitting. Different MLFNs are then regressed for different J values and the optimum J is then determined after considering accuracy, computational speed, and overfitting.

Due to the transfer function analytical form, S_k cannot be greater than α, i.e., 1.0. In addition, the regression is more efficient if all inputs and outputs are of the same order of magnitude: being the inputs of the order of some MPa for pressure and of some hundreds of K for temperature, this would slow down the regression and increase its sensitivity to local minima. The problem is overcome by introducing the reduced variables and compressing them through a proper compression function, before feeding the MLFN.

Generally speaking, it is:

$$U_i = u_i(V_i - V_{\min,i}) + A_{\min} \tag{8}$$

where

$$u_i = \frac{A_{\max} - A_{\min}}{V_{\max,\,i} - V_{\min,\,i}} \tag{9}$$

and

$$W_k = \exp\left[\frac{S_k - A_{\min}}{s_k} + g(W_{\min,\,k})\right] - 1 \tag{10}$$

where

$$s_k = \frac{A_{\max} - A_{\min}}{g(W_{\max,\,k}) - g(W_{\min,\,k})} \tag{11}$$

$$g(x) = \ln(x+1) \tag{12}$$

V_i is the physical input (T_r and/or ρ_r) and W_k is the physical output (η_r); $A_{\min}$ and $A_{\max}$ are the lower and upper ranges in which the physical inputs and output are compressed, and here they are set to 0.05 and 0.95. $V_{\min,\,i}$ and $V_{\max,\,i}$ are the limits of the independent input variables for the training set, and $W_{\min,\,k}$ and $W_{\max,\,k}$ are the limit values of the output dependent variable used in the training step. The quantity V_i is the independent variable, and W_k is the dependent variable.

Equations (2) to (12) represent the MLFN mathematical formalism and can be applied in sequential order.

The physical inputs are:

$$V_1 = T_r = T/T_c \qquad V_2 = \rho_r = \rho/\rho_c$$

and, similarly, the actual output W_1 represents the dependent variable,

$$W_1 = \eta_r(T_r, \rho_r) = \eta/\eta_c$$

Given an experimental data set of output S_k, in the independent variables U_i, the weighting factors are found by minimizing the following objective function by means of an optimization procedure:

$$f_{ob} = \frac{1}{\mathrm{NPT}} \sum_{i=1}^{\mathrm{NPT}} \left(\frac{\eta_i^{\mathrm{calc}} - \eta_i^{\mathrm{exp}}}{\sigma_i}\right)^2 \tag{13}$$

where NPT is the number of experimental points and σ_i is the claimed experimental uncertainty of each data set.

Once the training has been done, the viscosity equation is obtained in a continuous form. For further details about the characteristics of the MLFN applied, reference is made to the previous viscosity models for R123 [10] and R134a [11].

4. VISCOSITY NEURAL NETWORK EQUATIONS

4.1. Viscosity Explicit Equation

Since an MLFN is a mathematical function that links some inputs with some outputs, it seems reasonable to correlate viscosity data with the independent variables using this technique.

In Eqs. (2) to (12), considering that $I = 3$ and $K = 1$, it becomes

$$V_1 = T_r \qquad V_2 = \rho_r \qquad W_1 = \eta_r \tag{14}$$

where the reducing critical parameters are $T_c = 369.825$ K, $P_c = 4.248$ MPa, and $\rho_c = 220.48\ \text{kg}\cdot\text{m}^{-3}$. The viscosity reducing factor is $\eta_c = \frac{M^{1/2}P_c^{2/3}}{R^{1/6}N_A^{1/3}T_c^{1/6}} = 17.103\ \mu\text{Pa}\cdot\text{s}$ where $M = 44.098\ \text{kg}\cdot\text{kmol}^{-1}$ is the molar mass, R is the universal gas constant, and N_A is Avogadro's number. In the present work a MBWR 32-term equation of state from Younglove and Ely [17] is applied.

The viscosity data are generally classified as *primary* or *secondary*, and only the former ones are used in the correlation regression. The guidelines for the screening procedure are discussed in specialized textbooks, e.g., Ref. 14. In the present work the screening procedure adopted was as follows. We maintained as primary the data considered by Vogel et al. [9] as primary in developing their equation, even if they were measured at temperatures and pressures outside the validity range of their equation. We then tested all available 1577 experimental viscosity data versus the conventional equation and included all data with deviations less than 6%. We also included data that were not considered for the conventional equation, because they have appeared more recently. The data screened in this way were considered as *primitive*. Using these data, a first neural network version was regressed. After this preliminary screening, the first neural network was tested versus the *primitive* data. Neglecting the experimental points with deviations larger than 2%, a finer screening was done to identify the *primary* data, amounting to 969 in all, for which the final viscosity-MLFN equation was fitted. In Fig. 2 these data are presented in a T_r, P_r plane. After the data screening, the weighting factors of the MLFN equation (w_{ij} and w_{jk} matrices)—which are the new viscosity equation parameters for propane in a general form $\eta_r = \eta(\rho_r, T_r)$—can be obtained. With reference

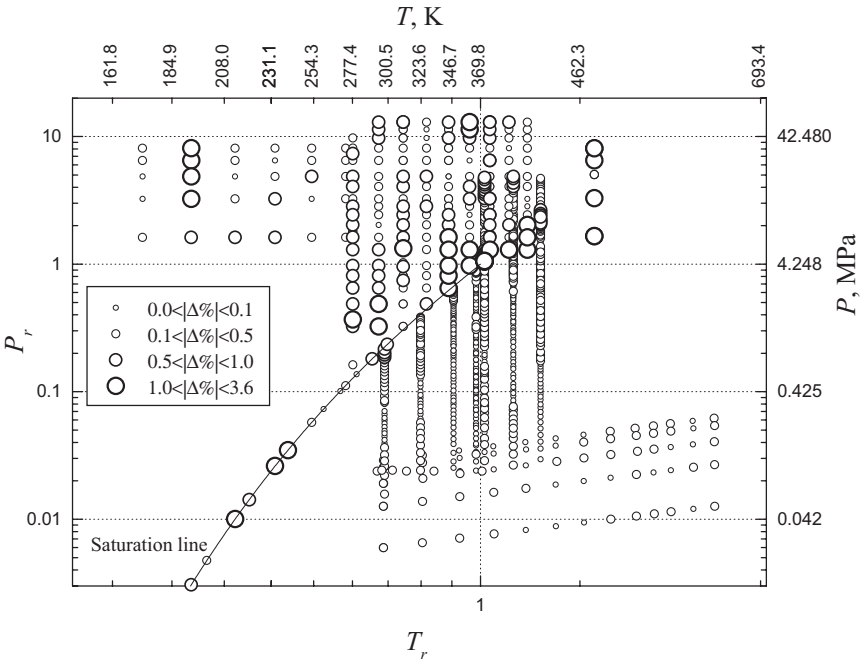

Fig. 2. Distribution of the propane primary data on the P_r, T_r plane. Error of the MLFN correlation.

to the previous paragraph, the optimum number of neurons in the hidden layer in this case is $J = 10$. The weighting factors are 30 for the first matrix w_{ij} and 11 for the second matrix w_{jk}, for a total of 41 weighting factors. The weighting factors as well as the other parameters and the residual error of the correlation are reported in Table I.

4.2. Viscosity Equations as Functions of Temperature and Pressure

In addition to considering a viscosity equation of the previous form,

$$\eta = \eta(\rho, T) \tag{15}$$

which has to be coupled with an equation of state for variable conversion, an equation system such as the one below could be written [21]:

$$\begin{cases} \eta = \eta(\rho, T) \\ P = P(\rho, T) \end{cases} \tag{16}$$

Table I. Parameters of the Viscosity MLFN Equations: $\eta_r = \eta_r(T_r, \rho_r)$ for the Overall Surface and $\eta_r = \eta_r(T_r, P_r)$ for the Liquid and for the Vapor Regions

i	j	Overall T_r, ρ_r w_{ij}	Liquid region w_{ij}	Vapor region w_{ij}
1	1	−1713.0600	−445.1590	−1037.7300
2	1	−1045.1800	2313.1700	171.0600
3	1	−698.8860	216.1800	−313.1420
1	2	1677.6000	−1737.5600	−281.6000
2	2	−1945.2600	331.4590	−42.9631
3	2	1682.6200	29.7240	90.0886
1	3	1294.5100	−257.8920	−4178.9500
2	3	536.4880	94.3698	975.5590
3	3	684.0470	108.7730	−3246.3200
1	4	−28.9535	−867.4630	−6558.5800
2	4	−522.6580	6113.5100	3051.5900
3	4	199.0630	402.8330	−2839.0600
1	5	372.8290	514.9170	−1319.1900
2	5	218.7270	−610.6200	421.4900
3	5	156.5680	−30.1998	−340.9980
1	6	153.2520	1196.8600	−3325.8700
2	6	685.2320	−1146.2300	−1161.1700
3	6	−112.9170	1063.6500	−3041.5100
1	7	−186.3270	658.7780	−2763.8900
2	7	637.8760	−4405.1300	340.6490
3	7	−668.6830	−228.9610	−2462.8600
1	8	−1191.9200	7346.8700	−4435.3500
2	8	−199.7620	−1825.9000	1337.9000
3	8	−481.6150	−56.9284	−3058.0500
1	9	−120.5360	1.28091	−5873.4100
2	9	−591.1310	307.5410	2080.1800
3	9	72.1437	−78.7515	−3462.7300
1	10	9298.3900	2698.5600	−4506.3700
2	10	−5334.3800	−798.9420	−3873.6400
3	10	4059.4600	−162.0800	−4463.9800

j	k	Overall T_r, ρ_r w_{jk}	Liquid region w_{jk}	Vapor region w_{jk}
1	1	−0.29518	1810.6900	−5747.6100
2	1	−1314.6200	−70.8132	−310.4120
3	1	−538.9390	−1083.6200	−241.8480
4	1	−421.3980	4079.4100	−1133.1500
5	1	1152.6500	−648.7840	3195.2200
6	1	2185.4800	−1634.8500	−310.4100
7	1	1114.8500	1837.6700	−176.7470
8	1	−113.9130	−3264.3900	−453.5870
9	1	2771.0200	−2021.7700	−933.0710
10	1	−3533.1200	−203.5590	−77.8700
11	1	2008.1600	1085.7400	28.3214

Parameter	Overall T_r, ρ_r	Liquid region	Vapor region
α	1	1	1
β	0.005	0.005	0.005
A_{min}	0.05	0.05	0.05
A_{max}	0.95	0.95	0.95
Bias 1	1.0	1.0	1.0
Bias 2	1.0	1.0	1.0
I	3	3	3
J	10	10	10
K	1	1	1
AAD training	0.29%	0.58%	0.22%

Parameter	Overall T_r, ρ_r	Liquid region	Vapor region
$V1_{min}$	$T_r = 0.2$	$T_r = 0.2$	$T_r = 0.7$
$V1_{max}$	$T_r = 1.8$	$T_r = 1.8$	$T_r = 1.8$
$V2_{min}$	$\rho_r = 0.0$	$P_r = 0.0$	$P_r = 0.0$
$V2_{max}$	$\rho_r = 4.0$	$P_r = 235.0$	$P_r = 1.0$
$W1_{min}$	$\eta_r = 0.4$	$\eta_r = 0.4$	$\eta_r = 0.4$
$W2_{max}$	$\eta_r = 800.0$	$\eta_r = 800.0$	$\eta_r = 2.0$

From this system a functional form $F(P, T, \eta) = 0$ could be derived, avoiding density as a variable and consequently not requiring the use of a high accuracy equation of state for the target fluid. From such F form, the three explicit functional forms can be extracted:

$$T = T(P, \eta) \tag{17}$$

$$P = P(T, \eta) \tag{18}$$

$$\eta = \eta(T, P) \tag{19}$$

which could be regressed by means of the former MLFN technique, still exclusively based on experimental data. These new functional forms are here named *viscosity equations of state* because they merge a viscosity equation and a thermodynamic equation of state.

Generally speaking, the form $T = T(P, \eta)$ for the whole surface has to be discarded due to the presence of viscosity minima for isobaric lines at near- and super-critical temperatures [11]. To follow such behavior, Eq. (17) would be forced to give two temperature solutions for the same viscosity value at the same pressure. Figure 3 shows isobaric lines: for propane viscosity minima are not experienced.

The form $P = P(T, \eta)$ cannot be generally applied for a similar reason; viscosity minima for the isothermal lines in the low-density vapor region may be encountered, depending on the single-fluid behavior. This form was

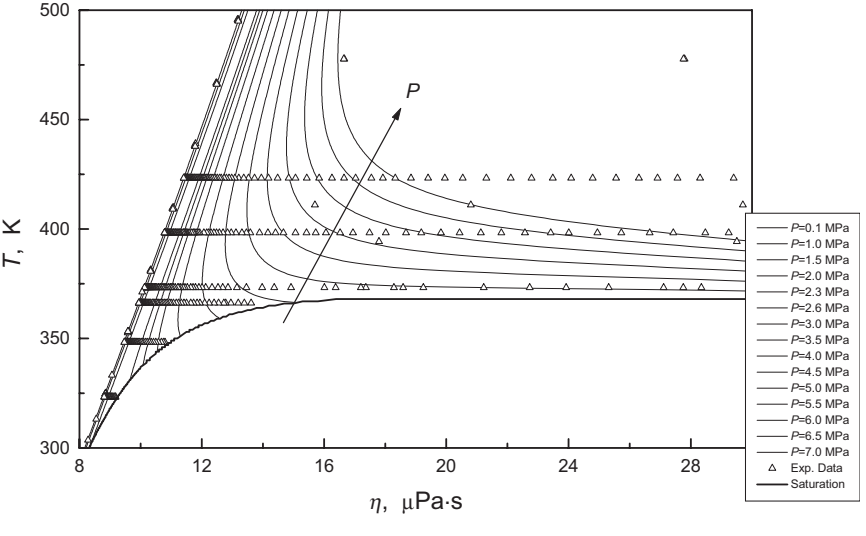

Fig. 3. Behavior of the MLFN viscosity model for the whole surface in an extended critical region.

Table II. Validation of the Viscosity MLFN Equations: $\eta_r = \eta_r(T_r, \rho_r)$ for the Whole Surface and $\eta_r = \eta_r(T_r, P_r)$ for the Liquid and for the Vapor Regions[a]

Ref.	Phase	T_{min} K	T_{max} K	P_{min} MPa	P_{max} MPa	ρ_{min} kg·m^{-3}	ρ_{max} kg·m^{-3}	Conventional eq. Bias %	Conventional eq. AAD %	Conventional eq. Max %	MLFN eq. Bias %	MLFN eq. AAD %	MLFN eq. Max %	MLFN eq. for liquid region Bias %	MLFN eq. for liquid region AAD %	MLFN eq. for liquid region Max %	MLFN eq. for vapor region Bias %	MLFN eq. for vapor region AAD %	MLFN eq. for vapor region Max %	NPT
										Primary data										
22	l	294	361	1.4	55.1	358.8	576.2	0.22	0.42	1.27	0.13	0.44	1.75	0.19	0.65	5.68				83
23	l	173	273	6.9	34.5	540.6	663.2	0.03	0.36	1.28	0.27	0.46	1.94	0.27	0.46	1.73				30
24	l	278	344	0.7	55.2	401.5	577.6	−0.33	0.44	1.34	−0.35	0.48	1.86	−0.29	0.57	2.39				51
25	l	278	278	1.5	31.2	524.9	567.5	−0.27	0.38	1.00	−0.09	0.51	1.04	−0.29	0.33	1.06				8
26	l	311	311	3.2	7.2	478.6	491.2	−0.32	0.71	1.19	−0.29	0.66	1.13	−0.27	0.53	0.96				5
23	sl	173	273	0.0	0.5	528.9	643.7	−0.34	0.35	0.83	−0.75	0.75	1.15	−0.41	0.41	0.90				6
27	sl	90	300	0.0	1.0	489.6	731.5	1.35	2.04	12.14	−0.08	0.80	3.34	−0.18	0.66	1.87				24
28	v	298	423	0.0	4.2	0.7	125.3	0.63	0.64	4.47	0.00	0.11	0.60				0.02	0.22	2.57	451
29	v	293	371	0.1	0.1	1.5	1.9	0.14	0.14	0.26	−0.08	0.13	0.24				−0.09	0.18	0.41	5
8	v	297	626	0.0	0.3	0.5	2.2	0.03	0.06	0.21	−0.03	0.14	0.34				−0.14	0.21	0.51	70
31	v	296	303	0.1	0.1	1.8	1.9	0.05	0.05	0.05	−0.23	0.23	0.23				−0.40	0.40	0.44	2
28	sc	373	423	4.3	20.7	73.2	446.4	1.92	1.92	7.72	0.22	0.43	3.59							163
24	sc	378	378	5.5	55.2	308.9	511.5	0.19	0.24	0.50	−0.52	0.57	2.26							13
22	sc	378	411	5.5	55.1	117.9	511.4	0.46	0.58	2.77	−0.45	0.57	3.10							39
25	sc	378	478	7.0	34.6	102.9	462.4	0.10	0.71	1.80	−0.40	0.87	2.02							19
Average		**90**	**626**	**0.0**	**55.2**	**0.5**	**731.5**	**0.67**	**0.80**	**12.14**	**−0.01**	**0.29**	**3.59**	**0.00**	**0.58**	**5.68**	**0.00**	**0.22**	**2.57**	**969**
										Secondary data										
27	l	90	300	1.7	31.5	494.3	740.4	6.35	6.57	14.99	−0.12	1.23	5.14	0.01	0.92	3.10				60
32	l	311	361	1.4	733.7	348.2	507.2	0.23	1.72	4.47	−0.10	1.91	6.11	0.35	1.78	4.89				36
33	l	298	348	2.8	34.5	387.4	552.3	−0.93	2.16	3.63	−1.00	1.91	3.41	−0.78	2.32	4.82				16
34	l	243	363	0.3	4.1	328.0	567.1	0.73	2.07	4.59	0.22	1.97	6.31	2.34	3.05	12.18				13
35	l	325	353	3.4	55.1	381.4	552.3	2.25	2.50	5.50	2.07	2.53	5.46	2.43	2.89	6.27				18
36	l	304	324	16.1	99.0	519.1	588.5	3.15	3.15	4.05	2.99	2.99	4.06	1.19	3.22	8.12				8
37	l	295	368	1.4	34.5	350.4	555.1	−0.49	3.52	22.00	−0.61	3.63	21.98	−0.60	3.82	21.50				55
38	l	88	363	0.3	3.9	334.6	733.7	−0.12	6.14	33.49	−1.41	5.36	22.49	−0.73	5.31	15.98				29
39	l	303	303	200.0	1000.0	649.2	793.1	−10.55	10.55	14.87	−8.68	8.68	9.93	−94.79	94.79	100.01				5
40	sl	112	176	0.0	0.0	640.9	707.7	2.06	2.28	5.40	1.43	1.77	4.53	1.79	2.04	5.08				5

32	sl	311	361	1.3	3.6	340.7	471.4	−3.02	3.02	6.29	−3.86	3.86	8.04	0.28	2.83	6.01				4
54	sl	84	170	0.0	0.0	647.4	739.0	6.33	10.85	18.73	0.52	5.57	18.50	−2.57	6.13	18.67				14
41	sl	200	289	0.0	0.7	506.8	615.6	−6.96	6.96	11.42	−7.33	7.33	11.45	−7.06	7.06	11.83				9
32	sv	328	361	1.9	3.6	43.0	108.8	−33.01	33.01	33.96	−35.15	35.15	36.94				−35.75	35.75	38.81	3
42	v	298	468	0.1	0.1	1.2	1.8	−0.49	0.49	0.87	−0.59	0.59	1.10				−0.75	0.75	0.99	5
43	v	298	468	0.1	0.1	1.2	1.8	−0.52	0.52	0.79	−0.60	0.60	1.03				−0.79	0.79	0.98	6
44	v	291	524	0.1	0.1	1.0	1.9	0.66	0.66	1.62	0.60	0.70	1.79				0.43	0.59	1.64	6
45	v	299	478	0.1	0.1	1.1	1.8	−0.65	0.65	0.91	−0.75	0.75	0.94				−0.91	0.91	1.25	5
55	v	313	313	0.1	0.1	1.7	1.7	−0.60	0.60	0.60	−0.87	0.87	0.87				−0.89	0.89	0.89	1
46	v	273	273	0.1	0.1	2.0	2.0	−0.68	0.68	0.68	−0.90	0.90	0.90				−1.22	1.22	1.22	1
25	v	278	478	0.1	3.6	1.8	72.4	−0.76	0.77	2.37	−1.02	1.03	4.41				−1.07	1.07	4.01	22
47	v	301	549	0.1	0.1	1.0	1.8	1.14	1.14	1.67	1.12	1.12	1.83				0.96	0.96	1.73	6
48	v	303	378	0.1	4.2	1.4	112.0	0.64	1.60	9.00	0.02	1.63	12.32				0.13	1.61	10.14	35
35	v	325	408	0.7	3.4	9.3	70.8	0.10	1.47	2.97	−0.50	1.65	5.14				−0.44	1.55	4.83	6
49	v	293	393	0.1	0.1	1.4	1.9	−1.53	1.53	2.08	−1.72	1.72	2.34				−1.76	1.76	2.37	6
24	v	278	378	0.1	4.1	1.4	105.4	−0.26	1.10	5.41	−1.06	1.81	5.16				−0.91	1.62	4.80	14
50	v	298	348	0.1	0.1	1.6	1.8	−1.80	1.80	1.97	−2.04	2.04	2.24				−2.05	2.05	2.44	3
22	v	294	411	0.7	4.1	9.3	105.2	−1.38	1.38	2.75	−2.29	2.29	4.52				−2.17	2.17	4.58	30
51	v	304	408	0.1	0.1	1.3	1.8	−2.34	2.34	3.31	−2.52	2.52	3.42				−2.53	2.53	3.49	11
52	v	308	364	0.1	0.1	1.5	1.8	−2.35	2.35	2.58	−2.56	2.56	2.77				−2.50	2.50	2.73	7
53	v	303	373	0.1	0.1	1.5	1.8	−2.54	2.54	2.92	−2.75	2.75	3.17				−2.71	2.71	3.11	8
54	v	373	373	0.1	0.1	1.5	1.5	−3.26	3.26	3.26	−3.39	3.39	3.39				−3.40	3.40	3.40	1
37	v	313	463	0.7	4.1	8.1	169.0	−1.20	4.60	45.14	−1.96	4.81	47.59				−2.12	5.09	56.46	32
33	v	398	498	2.8	2.8	31.9	45.7	−2.83	5.75	12.87	−3.11	5.97	13.63				−2.94	6.38	13.99	3
32	v	311	378	0.1	4.1	1.4	105.2	−10.93	11.54	28.30	−11.64	12.20	31.12				−11.56	12.13	31.54	42
36	sc	374	423	36.8	144.6	443.7	584.6	2.02	2.02	4.91	0.17	1.74	4.34							12
35	sc	380	408	6.9	55.1	195.9	509.3	1.31	2.05	5.42	0.59	1.85	4.44							16
33	sc	398	498	4.8	34.5	59.8	458.2	−3.60	4.42	11.03	−4.37	4.87	13.40							21
37	sc	388	463	5.2	34.5	74.6	467.7	8.42	8.44	18.45	7.47	7.78	16.36							24
32	sc	378	378	4.5	13.8	134.1	412.9	−5.08	8.55	21.98	−6.67	9.47	24.69							9
34	sc	370	370	4.3	4.3	264.4	264.4	28.41	28.41	28.41	24.64	24.64	24.64							1
Total																				**608**
Overall		**84**	**626**	**0.0**	**1000.0**	**0.5**	**793.1**	**−0.30**	**2.20**	**45.14**	**−0.61**	**1.68**	**47.59**	**−1.12**	**2.93**	**100.01**	**−1.11**	**1.54**	**56.46**	**1577**

[a] Phase: l = liquid, sl = saturated liquid, v = vapor, sv = saturated vapor, sc = supercritical.
Error: AAD = Average Absolute Deviation (%), Bias = bias (%), Max = maximum deviation (%); NPT = number of experimental points.

successfully developed for oxygen [21] with a different regression technique, because for that fluid the isothermal lines increase monotonically, not too steeply, and without minima.

The form $\eta = \eta(T, P)$ cannot be considered for the whole surface, because at saturation for a given T, $P^S(T)$ input couple the two viscosity values η^S_{liq}, η^S_{vap} have to be output. By separating the liquid region from the vapor region, two distinct equations of this form can be developed, one for each region, avoiding the inconsistency of the coexistence curve and also the viscosity minima representation difficulties.

Considering a case in which, for a target fluid, a high accuracy viscosity equation is required for only the liquid surface, where a sufficient amount of data is supposed to be available, but without disposing of the dedicated EoS for such fluid, the equation form (Eq. (19)) can be easily obtained. In this case the conventional method, Eq. (1), cannot be applied at all. Using the liquid data, an equation for the propane liquid surface is developed in the form of Eq. (19) demonstrating this further possibility of the proposed technique.

For the parallel case of the vapor region, the preceding problem can be similarly posed and a viscosity equation, with the form of Eq. (19), can be obtained directly from viscosity data, even if at low pressure they are not ordered along isotherms to allow the development of the conventional dilute-gas term [14]. In this case too, the dedicated EoS is not needed. The screening procedure for the two single-phase region equations leads to a classification of 207 and 528 primary data over a total of 479 and 781 points for the liquid and vapor regions, respectively. The supercritical region with both $T_r > 1$ and $P_r > 1$ can be similarly regressed, but it has not been done here for the sake of brevity.

4.3. Three Viscosity Equations: Parameters, Range of Validity, and Regression Residual Error

Following the preceding procedure, three MLFN have been obtained and their parameters are listed in Table I. For the viscosity equation $\eta(T, \rho)$ it is $V_1 = T_r$, $V_2 = \rho_r$, and $W_1 = \eta_r$, while for the two viscosity equations $\eta(T, P)$ it is $V_1 = T_r$, $V_2 = P_r$, and $W_1 = \eta_r$.

The validity ranges of the equations correspond to the primary data boundaries. For the viscosity equation of the $\eta = \eta(\rho, T)$ form, valid for the whole surface, they are $90 \leqslant T \leqslant 630$ K, $0 \leqslant \rho \leqslant 730\ \mathrm{kg \cdot m^{-3}}$, and $0 \leqslant P \leqslant 60$ MPa. For the viscosity equation of the $\eta = \eta(T, P)$ form, valid for the liquid region, the ranges are $90\ \mathrm{K} \leqslant T \leqslant T_c$ and $0 \leqslant P \leqslant 60$ MPa, whereas for the similar equation valid for the vapor region the ranges are

$90 \leqslant T \leqslant 630$ K and $0 \leqslant P \leqslant P_c$. In developing the two separate $\eta = \eta(T, P)$ equations, the whole surface has been subdivided by the coexistence line into two regions, excluding the supercritical region with both $T_r > 1$ and $P_r > 1$. The optimum number of neurons in the hidden layer for all three equations is $J = 10$. The weighting factors are 30 for the first matrix w_{ij} and 11 for the second one w_{jk}, for a total of 41 weighting factors. As reported in Table I, the residual error is, in all the cases, comparable to the experimental uncertainty.

5. VALIDATION OF THE NEW VISCOSITY EQUATIONS

The validation of the viscosity equations is reported in Table II together with comparisons with the conventional equation. The data are split into primary and secondary sets as previously discussed. The primary set has been used for the training step, and, consequently, the corresponding AADs are to be considered as the residual errors of the correlations.

The AAD for the $\eta(T, \rho)$ equation is 0.29%, that is, basically the experimental uncertainty of the data. The bias is −0.01%, showing then no systematic deviation is observed. The process of selecting the primary data and discarding the secondary results depending on the AAD, bias, and maximum deviation during the best fit of the MLFN, represents a powerful statistical data screening and it is one of the advantages of the present technique. On the other hand, for the same data, the AAD and bias of the conventional equation are, respectively, 0.80 and 0.67%. In Fig. 2 all the primary data with the residual error of the correlation are reported. The fact that some points with high deviations lay nearby some with very low deviations, suggests that the higher residual errors are due to experimental data uncertainty, rather than to a poor performance of the MLFN model.

The obtained accuracy on primary data for the two equations in the $\eta = \eta(T, P)$ form, the first for the liquid and the second for the vapor surfaces, show AAD values of 0.58 and 0.22%. The bias values of all three new equations, all very close to the zero line, indicate the absence of systematic shifting.

In the low-density vapor domain an inversion trend with respect to density has not been found for the obtained viscosity equation. In the region a considerable number of data is available, see Fig. 4, and the MLFN equation performs very well with respect to primary vapor data at low pressure, suggesting that the equation can be considered reliable in that region. In the same region some isotherms are shown in Fig. 4, to show that a wavy trend, typical of an overfitted equation with a high J value, does not occur.

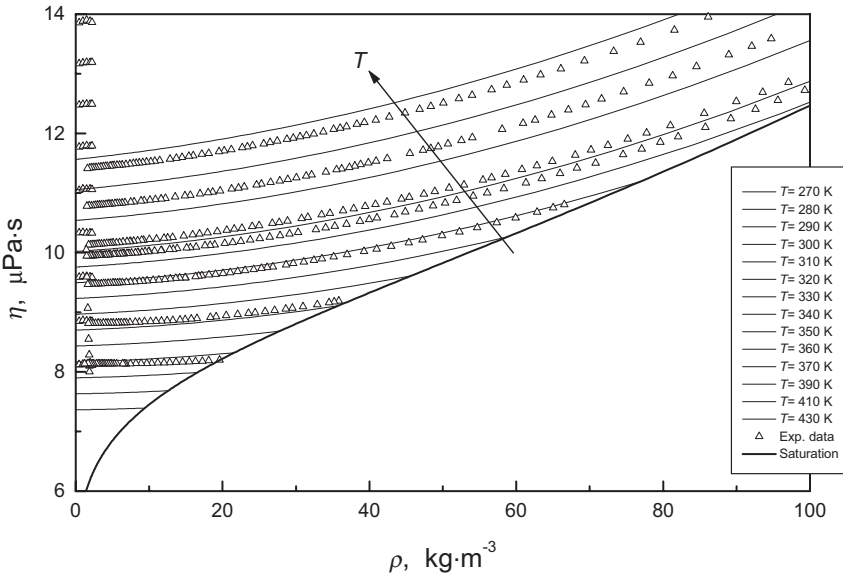

Fig. 4. Behavior of the MLFN viscosity model for the whole surface for the gas region with evidence that the locus of viscosity minima is not found.

6. ZERO-DENSITY LIMIT AND INITIAL DENSITY DEPENDENCE OF VISCOSITY

The viscosity of a pure vapor at lower densities may be represented by a density expansion truncated at the first power:

$$\eta(\rho, T) = \eta^{(0)}(T) + \eta^{(1)}(T)\,\rho + \cdots = \eta^{(0)}(T)[1 + B_\eta(T)\,\rho + \cdots] \quad (20)$$

In this equation the functions $\eta^{(0)}(T)$ and $\eta^{(1)}(T)$ are the zero-density and the initial density coefficients, whereas $B_\eta(T)$ is the second viscosity virial coefficient. Since at low density the terms raised to superior powers are negligible, $\eta^{(0)}(T)$ and $\eta^{(1)}(T)$ functions can be determined by fitting isothermal viscosity data at low density as a linear function of density. At each temperature the intercept and the slope of such straight lines represent the zero-density and the initial density coefficients. This has been done for propane, as reported in Fig. 5; low-density vapor data from Refs. 8 and 28 have been furthermore considered, limiting the points to $\rho \leqslant 10\,\mathrm{kg \cdot m^{-3}}$ leading to total of 218 data. The isothermal experimental data are fitted to

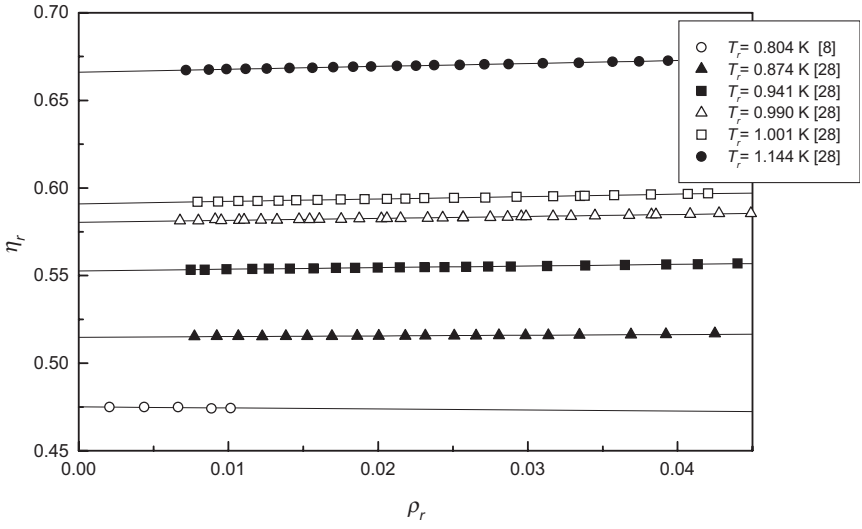

Fig. 5. Viscosity as a function of density for several isotherms: $\eta = \eta^{(0)} + \eta^{(1)}\rho$. Experimental data from Refs. 8 and 28.

a straight line, Eq. (20), to obtain $\eta^{(0)}$ and $\eta^{(1)}$ values at different temperatures, and finally to get the experimental viscosity second virial coefficient,

$$B_\eta(T) = \frac{\eta^{(1)}(T)}{\eta^{(0)}(T)} \tag{21}$$

Even though the procedure could seem to be trivial, some difficulties arise in evaluating $\eta^{(1)}$, i.e., the slope of the viscosity linear function. From Fig. 5 the linear fit seems to be carried out with a high degree of accuracy. If data from Ref. 8 are focused, for example, on isotherm $T_r = 0.804$, scattering is highlighted and the linear fit looks very poor, with an unacceptable correlation coefficient r^2 equal to 0.43. This affects, to a large extent, the slope evaluation and then $B_\eta(T)$. Figure 6 visually demonstrates this result. Looking at the y-axis scale in Fig. 6 and at the deviation from experimental data, then the maximum deviation is observed to be 0.063%, which is well below the uncertainty of any viscosity experimental techniques. Consequently, the following conclusion can be drawn: in order to evaluate the slope of low-density viscosity dependence and then $B_\eta(T)$, the required experimental accuracy appears to be greater than that currently available using the common experimental techniques.

It is possible to analyze the low-density behavior of the present MLFN equation in the $\eta = \eta(\rho, T)$ form, in terms of the $B_\eta(T)$ function. The second viscosity virial coefficient, Eq. (21), is analytically obtained from the

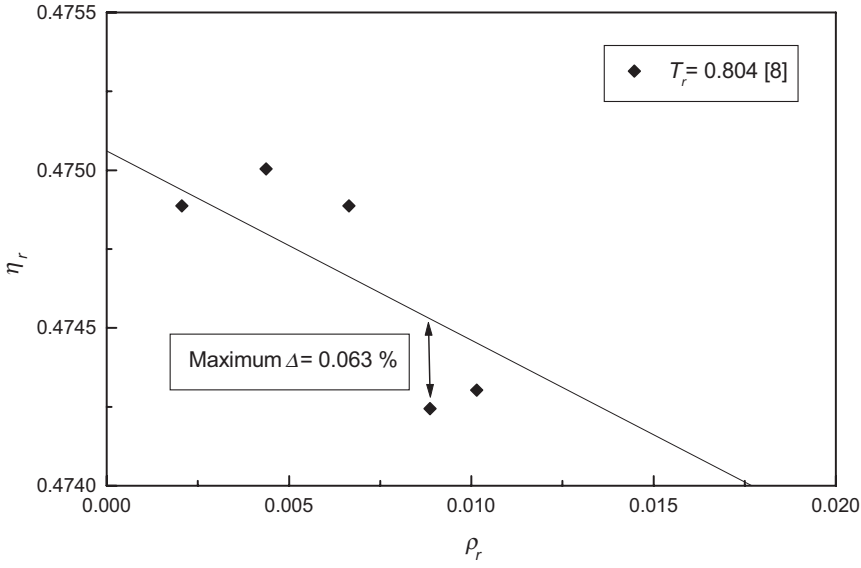

Fig. 6. Viscosity as a function of density for the $T_r = 0.804$ isotherm: $\eta = \eta^{(0)} + \eta^{(1)}\rho$. Experimental data from Ref. 8.

$\eta = \eta(\rho, T)$ MLFN equation imposing $\rho = 0$ to both the equation itself and its first derivative with respect to density, allowing the $\eta^{(0)}(T)$ and $\eta^{(1)}(T)$ functions to be generated. When validated on the 218 low-density experimental viscosity data, the MLFN equation gives AAD and bias values of 0.092 and −0.04%, respectively; the representation of the data themselves is then of very high quality. Comparing the AAD with the maximum deviation reported on Fig. 6, i.e., 0.063%, it becomes evident that in spite of being an absolutely reliable data correlation, the representation of slopes could not be as accurate as expected, because of the extremely high resolution required.

There is a third way for evaluating $B_\eta(T)$. The reduced viscosity second virial coefficient can be defined in the following way:

$$B^*_\eta(T^*) = \frac{B_\eta(T)}{N_A \sigma^3} \tag{22}$$

$$T^* = k_B T/\varepsilon \tag{23}$$

where ε/k_B and σ are the fluid dependent Lennard-Jones 12-6 potential parameters, while N_A is Avogadro's number. The parameters ε/k_B and σ are derived from the dilute-gas viscosity function $\eta^{(0)}(T)$ [8, 9, 14, 56, 57] and for propane it is $\varepsilon/k_B = 263.88$ K and $\sigma = 0.49748$ nm. The Rainwater

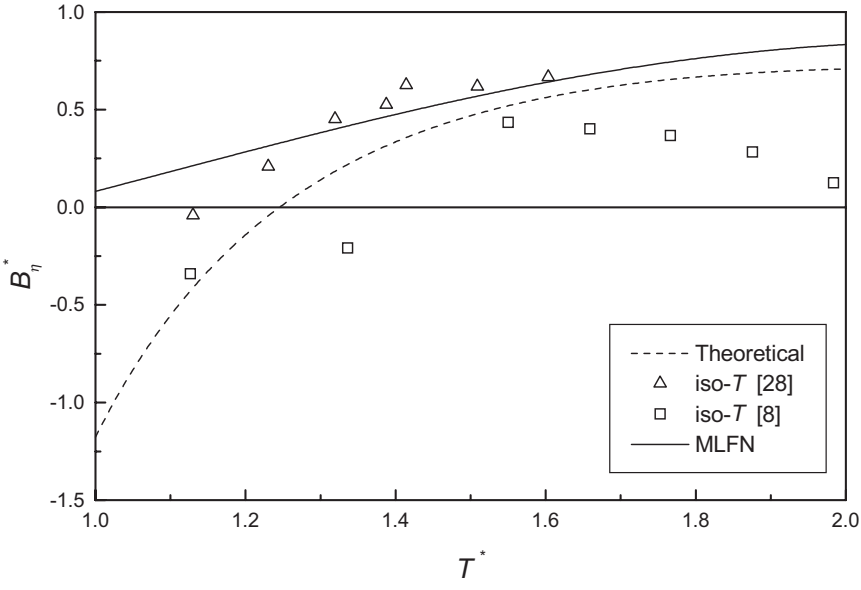

Fig. 7. Comparison of $B_\eta^*(T^*)$ as generated through experimental data, MLFN and theoretically sounded model. Experimental data from Refs. 8 and 28.

and Friend theory [56, 57] can be used to theoretically predict the $B_\eta^*(T^*)$ function, whose form has been recently enhanced by Vogel [8], Bich and Vogel [30], and then by Vogel et al. [9], recommending at last the following equation:

$$B_\eta^*(T^*) = \sum_{i=0}^{6} b_i (T^*)^{-0.25i} + b_7 (T^*)^{-0.25} + b_8 (T^*)^{-5.5} \tag{24}$$

$B_\eta^*(T^*)$ deduced from experimental data, the MLFN equation, and universal Eq. (24) are shown in Fig. 7.

Some comments can be drawn. First of all, the three approaches do not seem to match, reflecting the fact that high resolution is required to evaluate $B_\eta^*(T^*)$, as previously discussed. Even staying within data uncertainties of some parts per ten thousand, the low-density slope can be miscalculated. Data from Refs. 8 and 28 are considered primary and thus reliable, and the MLFN reproduce them within 0.092%, but this leads to significant different $B_\eta^*(T^*)$ values.

Secondly, Eq. (24) predicts negative values for $B_\eta^*(T^*)$, meaning that an inversion point occurs, i.e., along isotherms and approaching to zero

density, viscosity first decreases and then it starts to increase to $\eta^{(0)}(T)$. This is not shown by the MLFN. If Fig. 4 is considered, data seem to show that an inversion point does not occur. Viscosity could decrease and then increase in a span of some parts per ten thousand, a range that is lower than the resolution of experimental techniques and of MLFN accuracy. This does not seem to affect the value of the present work, since the deviations among different approaches is generated by deviations on data that are absolutely negligible on viscosity calculation. The MLFN could be forced to fit the first derivative of viscosity with respect to density, in order to represent the theoretical $B^*_\eta(T^*)$, but this is out of the scope of the work, which claims to rely solely on the data.

7. COST OF THE MODEL AND COMPARISON WITH OTHER MODELS

The following question should be posed: if the viscosity of a given fluid needs to be calculated, which approach should be chosen? The answer depends on the amount of information and of the time required both for setting up and running the model, i.e., on the cost of the model, and on the accuracy that needs to be reached.

The present MLFN $\eta = \eta(\rho, T)$ equation has been regressed on 969 experimental primary data. We tried to reduce this number, and we validated the resulting equation on the complete 969 data set. Results are reported in Table III. When less than half the data are considered, MLFN is not able to represent the viscosity surface. As a rule of thumb, MLFN should only be considered for representing the whole surface when few hundreds of data are available. In addition, extrapolation where data are lacking is not reliable.

MLFN has been also used for representing viscosity in the framework of an extended corresponding state approach [58, 59]. Using a few tens of data, an uncertainty of around 1.0% can be attained [58]. Consequently, depending on the target accuracy and on the available data, one of the two

Table III. Performance of Viscosity MLFN as Function of Number of Experimental Data

NPT for MLFN training	Residual training error %	Deviation on total 969 primary data %	Maximum deviation on total primary data %
969	0.29	0.29	3.59
512	0.43	0.52	5.48
256	0.59	153.0	24251.0

Table IV. Comparisons between Viscosity Models

Model	Input	Accuracy	Advantages	Disadvantages
Conventional equation [9, 14]	– Few hundreds of data – EoS for conversion of variables	0.8 to 2.7%	– Accuracy – Moderate extrapolation allowed	– Data reduction required for the three contributions regression – Not applicable to a limited region – Rigid analytical form sometimes does not allow to be spread on data
MLFN equation in T, ρ [present work, 10–13]	– Few hundreds of data – Eq. of state for conversion of variables	0.3%	– Accuracy – Straightforward from data – Applicable to a limited region – Flexibility	– No extrapolation allowed
MLFN equation in T, P [present work, 10–13]	– Few hundreds of data	0.3%	– Accuracy – Straightforward from data – Applicable to a limited region – Flexibility – No Eq. of state required	– No extrapolation allowed
MLFN applied to extended corresponding states [58, 59]	– Few tens of data – EoS for a reference fluid – Viscosity equation for a reference fluid	1.0%	– Few input needed – Straightforward from data – Applicable to a limited region – Flexibility	– Chemical similitude (conformality) with a well known reference fluid required
Three parameter corresponding states [1-6]	– EoS for two reference fluids – Viscosity eq. for two reference fluids	1.0 to 2.0%	– Predictive	– Conformality with two well known reference fluids required – Accuracy

approaches can be chosen. In Table IV a comparison between models is presented, to provide guidelines about which technique can be selected for viscosity calculations.

8. CONCLUSIONS

A new method based on the *multilayer feedforward network* technique has been proposed for the development of a conventional viscosity equation and has been applied to propane, for which a former conventional equation was available. The method is completely correlative and based directly on the available viscosity data. Three viscosity explicit functions are proposed here; the first is in the ρ, T variables and the other two are in the P, T variables, one for only the liquid region and the other for only the

vapor region. These last two equations do not require a high accuracy equation of state for conversion of the variables. The accuracies of the three new MLFN viscosity equations with respect to primary data present AAD values ranging from 0.22 to 0.58%. A validation of the conventional equation with respect to the present data sets gives an uncertainty of 0.67% on the 969 primary data.

The initial density dependence, as derived from the present model, is in substantial agreement, within the limits of the data accuracy in that region, with the theoretical predictions of the reduced second viscosity virial coefficient.

Considering the heuristic and non-theoretically founded nature of the method, it can be furthermore used as a powerful tool for experimental data screening. The neural networks represent promising tools for viscosity equation development, being able to represent the whole viscosity surface well within the uncertainty of the experimental data.

REFERENCES

1. A. S. Teja and P. A. Thurner, *Chem. Eng. Commun.* **49**:79 (1986).
2. B. Willman and A. S. Teja, *Chem. Eng. J.* **37**:65 (1988).
3. K. J. Okeson and R. L. Rowley, *Int. J. Thermophys.* **12**:119 (1991).
4. G. Scalabrin and M. Grigiante, presented at *13 th Symp. Thermophys. Properties*, Boulder, Colorado (1997).
5. G. Cristofoli, M. Grigiante, and G. Scalabrin, *High Temp.-High Press.* **33**:83 (2001).
6. G. Scalabrin, G. Cristofoli, and M. Grigiante, *Int. J. Energy Research* **26**:1 (2002).
7. M. O. McLinden, S. A. Klein, E. W. Lemmon, and A. P. Peskin, *NIST Standard Reference Database 23, Version 6.0*, (REFPROP) (1998).
8. E. Vogel, *Int. J. Thermophys.* **16**:1335 (1995).
9. E. Vogel, C. Küchenmeister, E. Bich, and A. Laesecke, *J. Phys. Chem. Ref. Data* **27**:947 (1998).
10. G. Scalabrin, C. Corbetti, and G. Cristofoli, *Int. J. Thermophys.* **22**:1383 (2001).
11. G. Cristofoli, L. Piazza, and G. Scalabrin, *Fluid Phase Equilib.* **199**:223 (2002).
12. G. Scalabrin, L. Piazza, and V. Vesovic, *High Temp.-High Press.* **34**:457 (2002).
13. G. Scalabrin and G. Cristofoli, *Int. J. Refrig.* **26**:302 (2003).
14. J. Millat, J. H. Dymond, and C. A. Nieto de Castro, *Transport Properties of Fluids* (Cambridge Univ. Press, United Kingdom, 1996).
15. G. A. Olchowy and J. V. Sengers, *Phys. Rev. Lett.* **61**:15 (1988).
16. J. Luettmer-Strathmann, J. Sengers, and G. Olchowy, *J. Chem. Phys.* **103**:7482 (1995).
17. B. A. Younglove and J. F. Ely, *J. Phys. Chem. Ref. Data* **16**:577 (1987).
18. G. Cybenko, *Mathematics of Control, Signals, and Systems* **2**:303 (1989).
19. K. Hornik, M. Stinchcombe, and H. White, *Neural Networks* **2**:359 (1989).
20. V. Kurkova, *Neural Networks* **5**:501 (1992).
21. A. Laesecke, R. Krauss, K. Stephan, and W. Wagner, *J. Phys. Chem. Ref. Data* **19**:1089 (1990).
22. K. E. Starling, B. E. Eakin, and R. T. Ellington, *AIChE J.* **6**:438 (1960).
23. E. T. S. Huang, G. W. Swift, and F. Kurata, *AIChE J.* **12**:932 (1966).

24. J. G. Giddings, J. T. F. Kao, and R. Kobayashi, *J. Chem. Phys.* **45**:578 (1966).
25. L. T. Carmichael, V. M. Berry, and B. H. Sage, *J. Chem. Eng. Data* **9**:411 (1964).
26. H. J. Strumpf, A. F. Collings, and C. J. Pings, *J. Chem. Phys.* **60**:3109 (1974).
27. D. E. Diller, *J. Chem. Eng. Data* **27**:240 (1982).
28. J. Wilhelm and E. Vogel, *J. Chem. Eng. Data* **46**:1467 (2001).
29. R. Wobser and F. Mueller, *Kolloid-Beih.* **52**:165 (1941).
30. E. Bich and E. Vogel, in *Transport Properties of Fluids*, J. Millat, J. H. Dymond, and C. A. Nieto de Castro, eds. (Cambridge Univ. Press, United Kingdom, 1996), pp. 72–82.
31. J. Kestin, S. T. Ro, and W. A. Wakeham, *Trans. Faraday Soc.* **67**:2308 (1971).
32. B. H. Sage and W. N. Lacey, *Ind. Eng. Chem.* **30**:829 (1938).
33. L. B. Bicher, Jr. and D. L. Katz, *Ind. Eng. Chem.* **35**:754 (1943).
34. G. W. Swift, J. Lohrenz, and F. Kurata, *AIChE J.* **6**:415 (1960).
35. J. D. Baron, J. G. Roof, and F. W. Wells, *J. Chem. Eng. Data* **4**:283 (1959).
36. W. R. Van Wijk, J. H. van der Veen, H. C. Brinkman, and W. A. Seeder, *Physica* **7**:45 (1940).
37. A. S. Smith and G. G. Brown, *Ind. Eng. Chem.* **35**:705 (1943).
38. G. W. Swift, A. J. Christy, and F. Kurata, *AIChE J.* **5**:98 (1959).
39. S. E. Babb, Jr. and G. J. Scott, *J. Chem. Phys.* **40**:3666 (1964).
40. G. I. Galkov and S. F. Gerf, *Zh. Tekh. Fiz.* **11**:613 (1941).
41. M. R. Lipkin, J. A. Davison, and S. S. Kurtz, Jr., *Ind. Eng. Chem.* **34**:976 (1942).
42. Y. Abe, J. Kestin, H. E. Khalifa, and W. A. Wakeham, *Physica A* **93**:155 (1978).
43. Y. Abe, J. Kestin, H. E. Khalifa, and W. A. Wakeham, *Ber. Bunsenges. Phys. Chem.* **83**:271 (1979).
44. M. Trautz and K. G. Sorg, *Ann. Phys.* **10**:81 (1931).
45. J. Kestin, H. E. Khalifa, and W. A. Wakeham, *J. Chem. Phys.* **66**:1132 (1977).
46. A. Klemenc and W. Remi, *Monatsh. Chem.* **44**:307 (1923).
47. M. Trautz and F. Kurz, *Ann. Phys.* **9**:981 (1931).
48. E. W. Comings, B. J. Mayland, and R. S. Egly, *Univ. Illinois Eng. Exptl. Sta. Bull.* **354**:1 (1944).
49. T. Titani, *Bull. Chem. Soc. Japan* **5**:98 (1930).
50. K. Nagaoka, Y. Yamashita, Y. Tanaka, H. Kubota, and T. Makita, *J. Chem. Eng. Japan* **19**:263 (1986).
51. M. Diaz Pena and J. A. R. Cheda, *Anal. Quim. (Esp.)* **71**:34 (1975).
52. J. D. Lambert, K. J. Cotton, M. W. Pailthorpe, A. M. Robinson, J. Scrivins, W. R. F. Vale, and R. M. Young, *Proc. Roy. Soc. London Ser.* **A231**:280 (1955).
53. H. Adzumi, *Bull. Chem. Soc. Japan* **12**:199 (1937).
54. S. F. Gerf and G. I. Galkov, *Zh. Tekh. Fiz.* **10**:725 (1940).
55. H. Senftleben and H. Gladish, *Z. Phys.* **125**:653 (1949).
56. D. G. Friend and J. C. Rainwater, *Chem. Phys. Lett.* **107**:590 (1984).
57. J. C. Rainwater and D. G. Friend, *Phys. Rev. A* **36**:4062 (1987).
58. G. Scalabrin, G. Cristofoli, and D. Richon, *Fluid Phase Equilib.* **199**:265 (2002).
59. G. Scalabrin, G. Cristofoli, and D. Richon, *Fluid Phase Equilib.* **199**:281 (2002).
60. H. Miyamoto and K. Watanabe, *Int. J. Thermophys.* **21**:1045 (2000).